Eur Biophys J (2009) 39:139–148
DOI 10.1007/s00249-009-0456-7

ORIGINAL PAPER

# Erythrocyte orientational and cell volume effects on NMR *q*-space analysis: simulations of restricted diffusion

**Timothy J. Larkin · Philip W. Kuchel**

Received: 3 February 2009 / Revised: 26 March 2009 / Accepted: 7 April 2009 / Published online: 28 April 2009


**Abstract** Pulsed field-gradient spin echo nuclear magnetic resonance spectroscopy of water diffusing in erythrocytes leads to diffusion interference and diffraction effects, which are visualised in *q*-space plots of signal intensity versus the magnitude of the spatial wave-number vector **q**. Interpretation of the features of these *q*-space plots has been aided by Monte Carlo random walk simulations of diffusion in lattices of virtual erythrocytes. Here, the effect of varying the orientation of the cells with respect to the direction in which diffusion is measured, on the appearance of *q*-space plots, was investigated, together with the effect of changing the cell volume. We show that these changes are reflected in the appearance of the plots in a way that is diagnostic of the microscopic geometry of the sample.

**Keywords** Monte Carlo · Nuclear magnetic resonance · Pulsed field-gradient spin echo · *q*-Space plot · Red blood cell

**Abbreviations**

| | |
|---|---|
| Ht | Haematocrit |
| MCV | Mean cell volume |
| NMR | Nuclear magnetic resonance |
| PGSE | Pulsed field-gradient spin echo |
| RBC | Red blood cell |
| RDW | Red cell distribution width |

"Proteins, membranes and cells: the structure-function nexus". Contributions from the annual scientific meeting (including a special symposium in honour of Professor Alex Hope of Flinders University, South Australia) of the Australian Society for Biophysics held in Canberra, ACT, Australia, September 28 to October 1, 2008.

T. J. Larkin · P. W. Kuchel (✉)
School of Molecular and Microbial Biosciences,
University of Sydney, Building G08,
Sydney, NSW 2006, Australia
e-mail: p.kuchel@mmb.usyd.edu.au

## Introduction

The aim of this work was to investigate the effect of orientation on the *q*-space plots produced from nuclear magnetic resonance (NMR) pulsed field-gradient spin echo (PGSE) diffusion measurements on a cellular system. Avram et al. (2004, 2008) have shown both experimentally and theoretically for diffusion of water in cylinders that have a large length to diameter ratio the appearance of resulting *q*-space plots is highly dependent on the cylinder orientation, with even small deviations resulting in a Gaussian decay of the signal. This is in contrast to simulated results in oriented cylinders of finite length where diffraction minima are seen for all orientations (Söderman and Jonsson 1995).

The cellular system chosen for our study was the human red blood cell (RBC) due to the well-defined *q*-space plots that can be obtained as a result of the alignment of the cells within the uniform magnetic field of an NMR magnet (Kuchel et al. 1997, 2000). However, this alignment may be expected to be incomplete, especially for suspensions with a low packing density (haematocrit, Ht), or a very high one. The effect of cell orientation on the form of *q*-space plots from suspensions of RBCs has been considered previously (Jiang et al. 2001), but using a flat cylinder as the model of an RBC. However, here, we investigated these effects using RBCs modelled more realistically as biconcave discs, or discocytes.

In addition, previous simulations of water diffusion in RBCs had been based on a lattice of cells with uniform

volume (Regan and Kuchel 2000, 2002, 2003a, b); but real RBCs from a single donor have a distribution of volumes and hence a distribution of mean cell diameters (Price-Jones 1929). The effect of variation of cell volume on the appearance of $q$-space plots from samples of RBCs was also investigated using random walk simulations of diffusion.

Translational displacement is measured in PGSE-NMR spectroscopy by encoding spatial information in the phase of nuclear spins by the application of magnetic field-gradient pulses. This enables the calculation of diffusion coefficients (Stejskal and Tanner 1965). When diffusion is impeded by a confining geometry, it can give rise to interference and diffraction-like effects due to spatial coherences of the magnetisation phases in the sample. These diffraction-like effects have been observed in solids (Mansfield and Grannell 1973). On the other hand, the Fourier transform of a $q$-space plot derived from a suspension of yeast cells yields a Gaussian average propagator that reflects the wide size distribution of the yeast cells (Cory and Garroway 1990); the size dispersion is so large that actual diffraction-like patterns are not seen in the resulting $q$-space plots. However, if a porous system has a certain level of regularity of size, $q$-space plots can show interference-like features that when appropriately analysed provide information on the structure and pore size of the network (Callaghan et al. 1991).

Diffusion-coherence effects are readily observed from suspensions of human RBCs using plots of the normalised signal intensity versus the spatial wave-number vector $\mathbf{q}$ (units, $\mathrm{m}^{-1}$):

$$\mathbf{q} = (2\pi)^{-1}\gamma\delta\mathbf{g} \tag{1}$$

where $\gamma$ is the magnetogyric ratio, $\delta$ is the duration of the magnetic field-gradient pulses applied during the PGSE experiment, and $\mathbf{g}$ is the magnetic field-gradient vector.

PGSE experiments on the diffusion of water in suspensions of RBCs produce $q$-space plots with a number of well-defined features. The first of these is a 'pore-hopping shoulder', a diffusion interference effect due to water moving in the extracellular medium, followed by several diffraction minima arising from the restricted diffusion of water inside the cells (Torres et al. 1999). An understanding of the factors that influence the appearance of the $q$-space plots derived from suspensions of RBCs has been aided by the use of extensive computer simulations of diffusion in lattices of virtual cells (Regan and Kuchel 2002). This previous work has investigated the effect of membrane permeability (Regan and Kuchel 2003b), and the effect of various lattice arrangements of the cells (Regan and Kuchel 2003a).

The analysis of data from $q$-space plots of water diffusing in RBCs has been aided by the development of a data-processing method based on the Fourier transform of the second derivative following application of a Blackman-Harris digital filter (Kuchel et al. 2004). This method enhances the features of the $q$-space plot and yields information about the compartment sizes where the restricted diffusion occurs, through the Fourier relationship between the attenuation of the NMR signal in PGSE experiments and the average propagator. The method has recently been applied to follow systematic, predictable shape changes in RBCs (Pages et al. 2008).

## Theory of methods

### Monte Carlo random walk

The method used for the random walk simulations has been described previously (Regan and Kuchel 2000, 2002, 2003a, b) and for completeness is briefly described here: it involves diffusion on a cubic lattice where for each time step a particle moves one jump length in the $\pm x$-, $\pm y$- and $\pm z$-directions as determined using a random binary digit. The jump length is derived from the Einstein formula:

$$s = \sqrt{2Dt} \tag{2}$$

where $D$ is the diffusion coefficient of the particle and $t$ is the time for a single jump. While a Monte Carlo random walk was chosen for our investigations, a second method for simulating diffusion using a matrix formalism is available (Callaghan 1997); however, it requires an analytical solution to the boundary-value diffusion problem, making it more suited to modelling diffusion in compartments that can be represented by simple geometries such as parallel planes, cylinders and spheres.

### Erythrocyte model

RBCs were modelled using a degree-4 surface that approximates the shape of a human RBC (Fig. 1a). The surface for an RBC aligned with the magnetic field is described by the equation (Kuchel and Fackerell 1999):

$$\left(x^2 + y^2 + z^2\right)^2 + P\left(x^2 + y^2\right) + Q\left(z^2\right) + R \tag{3}$$

where $P$, $Q$ and $R$ are constants related to the dimensions of the biconcave disk:

$$\begin{aligned} P &= -\frac{d^2}{2} + \frac{a^2}{2}\left(\frac{d^2}{b^2} - 1\right)\left(1 - \frac{b^2}{a^2}\right)^{1/2} \\ Q &= \frac{d^2}{b^2}P + \frac{b^2}{4}\left(\frac{d^4}{b^4} - 1\right) \\ R &= -\frac{d^2}{4}P - \frac{d^4}{16} \end{aligned} \tag{4}$$

Here, $a$ is the maximum thickness, $b$ is the minimum thickness, and $d$ is the main diameter (Fig. 1a). Equation 3

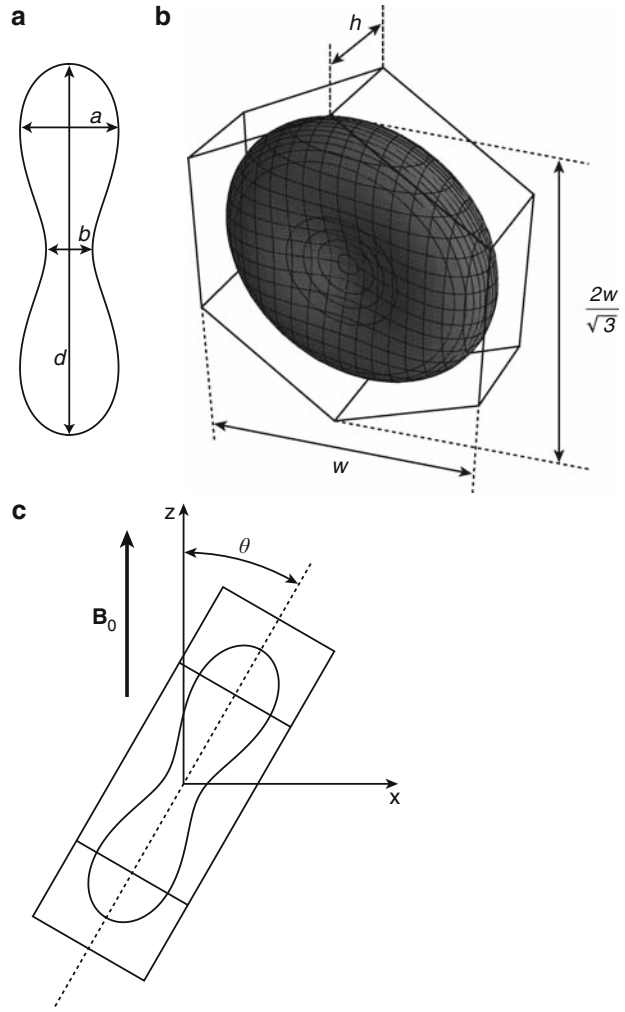


**Fig. 1** **a** Schematic of a cross-section through the model RBC used for the simulations: $a$ is the maximum thickness of the erythrocyte, $b$ is the minimum thickness, and $d$ is the main diameter of the cell. **b** Represents the unit cell used in the simulations, consisting of an RBC inside a hexagonal prism. The dimensions of the prism are shown with $w$ being the width, and $h$ the depth of the prism. **c** Shows how the orientation of the RBC ($\theta$) with respect to the external magnetic field $\mathbf{B}_0$ was defined

was modified to make the surface rotatable about both the $y$- and $z$-axes by the angles $\theta$ and $\psi$, respectively, to become:

$$\begin{aligned}&\Big[(z\sin\theta+\cos\theta(x\cos\psi-y\sin\psi))^2+(y\cos\psi+x\sin\psi)^2\\&\quad+(z\cos\theta-\sin\theta(x\cos\psi-y\sin\psi))^2\Big]^2\\&\quad+P\Big[(y\cos\psi+x\sin\psi)^2\\&\quad+(z\cos\theta-\sin\theta(x\cos\psi-y\sin\psi))^2\Big]\\&\quad+Q(z\sin\theta+\cos\theta(x\cos\psi-y\sin\psi))^2+R\end{aligned}\tag{5}$$

The purpose of the rotation about the $y$-axis was to change the orientation of the model cell with respect to the external magnetic field, which is, by definition, along the $z$-axis. The rotation of the cell about the $z$-axis was done to average the signal when gradients were applied along the $x$- and $y$-axes; this accounts for the random orientation of RBCs that occurs about the $z$-axis in a real sample.

The model RBC was placed inside a regular hexagonal prism (Fig. 1b) to generate the unit cell that was then used in the simulations. The unit cell allowed ready description of the transmembrane exchange of water and used periodic boundary conditions at the prism surfaces. The hexagonal prism was also rotated about the $y$- and $z$-axes. The dimensions of the prism were determined by fixing its volume ($V_{\text{prism}}$) with respect to the volume of the cell ($V_{\text{cell}}$) using:

$$V_{\text{prism}} = V_{\text{cell}}/H_{\text{t}} \tag{6}$$

where $V_{\text{prism}}$ is given by

$$V_{\text{prism}} = w^2 h \sin(\pi/3) \tag{7}$$

## Membrane transition probability

The red cell membrane is semi-permeable to water, and to account for this in the simulations it is necessary to define the probability of a particle actually transiting the membrane ($t_{\text{p}}$) if a jump takes it across the cell boundary. This probability is calculated using the relationship (Regan and Kuchel 2000):

$$t_{\text{p}} = P_{\text{d}} s_{\text{in/out}}/D_{\text{in/out}} \tag{8}$$

where $P_{\text{d}}$ is the membrane permeability, $s_{\text{in/out}}$ is the jump length of the particle inside or outside the RBC and $D_{\text{in/out}}$ is the diffusion coefficient of the particle inside or outside the RBC, which ever is relevant.

## NMR signal

During the gradient pulses of the PGSE diffusion experiment, a spin acquires an additional phase angle ($\varphi$) that depends on its spatial position and the strength of the magnetic field-gradient pulse. In a Monte Carlo random walk simulation, the value of $\varphi$ is updated after each jump using the equation:

$$\varphi(\mathbf{g}) = \gamma \mathbf{g} t |\mathbf{r}| \tag{9}$$

where $t$ is the duration of a jump, and $|\mathbf{r}|$ is the magnitude of the position vector of the particle with respect to the applied magnetic field gradient. During the first gradient pulse, phase is accumulated or lost, while during the second gradient pulse the acquired phase has the opposite sign. The accumulated phase angle at the end of the second gradient pulse is then converted into signal intensity ($E$) by taking the projection of the magnetisation vector onto the $-y$-axis, using the expression:

$$E(\mathbf{g}) = \cos(\varphi)\mathbf{g} \tag{10}$$

## Methods

### Experimental

To determine the volume distribution of a sample of RBCs, fresh blood was obtained from the cubital fossa of a healthy donor (T.J. Larkin). The mean cell volume (MCV) and red cell distribution width (RDW) for this sample were measured in triplicate using a Sysmex KH-21 (Sysmex, Kobe, Japan) haematology analyser.

### Simulation programs

The Monte Carlo random walk simulation programs were written in a combination of *Mathematica* 6.0 (Wolfram, Champaign, IL, USA) and C. *Mathematica* has a library of C functions that enable communication between it and an external C program. The Monte Carlo method involves the generation of large numbers of random binary and floating-point numbers. *Mathematica* generated these numbers (using a cellular automaton-based generator) that were then passed to the C program that performed the actual simulation. The intersection of a particle with the surface describing the RBC involved the solution of a quartic equation: expressions for the coefficients of the quartic were generated using *Mathematica*. (They are not given here due to their length and complexity but are available on request from the authors.) The solution to the boundary problem was achieved by calculating the coefficients of the quartic in the C program and passing these to a custom-made function in *Mathematica* that used the built in function Solve. The real, calculated roots of the quartic were then passed back to the C program. Starting positions of the point molecules were assigned randomly either inside or outside the RBC in the unit cell, weighted according to the relative intra- and extracellular volumes, i.e., the Ht of the RBC suspension. The output of the C program was a list of gradient strengths and corresponding signal intensities that were returned to the main *Mathematica* program for subsequent signal analysis and graphing.

### Simulation parameters

The experimental PGSE-NMR parameters used in the simulations were chosen to be consistent with those used previously (Regan and Kuchel 2000, 2002, 2003a, b), being a diffusion time ($\Delta$) of 20 ms, gradient pulse duration ($\delta$) of 2 ms, giving a total simulated time of 22 ms. The gradient magnitude ($g$) was varied between 0 and 10 $Tm^{-1}$ in 96 equally spaced steps, and the proton magnetogyric ratio ($\gamma$) of $2.62752 \times 10^8$ rad $T^{-1}$ was used. The permeability of the RBC membrane, $P_d$, was set to $6.1 \times 10^{-5}$ m $s^{-1}$ which is the experimentally determined value for human RBCs (Benga et al. 1990). Diffusion coefficients of water were $8.0 \times 10^{-10}$ and $1.6 \times 10^{-9}$ $m^2$ $s^{-1}$, inside and outside the RBC, respectively. The dimensions of the RBC for simulations involving only changes in the orientation of the cell were $a = 2.12 \times 10^{-6}$ m, $b = 1.0 \times 10^{-6}$ m, and $d = 8.0 \times 10^{-6}$ m. These values gave an RBC volume of 86 fl which is the mean value for human RBCs (Dacie and Lewis 1975). To generate RBCs with volumes of 76 and 96 fl, $d$ was set to $7.525 \times 10^{-6}$ and $8.45 \times 10^{-6}$ m, respectively, while using the same values of $a$ and $b$. These volumes were chosen as they represent the extreme values expected for normal human RBCs (Price-Jones et al. 1935). The surface area for cells with each of the volumes was calculated by summing the areas of the triangles used to plot the surface generated by Eqs. 3 and 4 in *Mathematica*. The values obtained were 115.2 $\mu m^2$ for 76 fl cells, 127.9 $\mu m^2$ for 86 fl cells and 140.7 $\mu m^2$ for 96 fl cells, with the surface areas of the 76 and 96 fl cells differing by 10% from that of the 86 fl cells. All the simulations were performed using an Ht of 0.5 and with $10^6$ particles. The rotation of the cell about the $y$-axis to average the signal intensities obtained from gradients applied along the $x$- and $y$-axes was implemented by performing the simulation in packets of 1,000 particles. For each particle in a packet, the value of $\varphi$ was incremented by 0.18° to give a total rotation of the cell of 180°.

For simulations where the orientation of the cell was varied, the values of $\theta$ used were, 0° (aligned with the external field), 10°, 30°, 45°, 60° and 90°. A simulation where the orientation $\theta$ was randomly chosen to be an integer value between 0° and 6° for each particle was also carried out, with the values of $\theta$ chosen with uniform weighting.

To represent a real suspension of RBCs, a simulation where the cells were given a random volume was constructed. For each particle, a random RBC volume was sampled from a normal distribution of a mean of 86 fl (Dacie and Lewis 1975), and standard deviation of 5 fl (for explanation of this choice of standard deviation see "Results"). A table of cell diameter $d$ values and corresponding prism dimensions $w$ and $h$ was constructed to give volumes between 71 and 101 fl (mean ± 3SD) in 0.25 fl steps, and a set of values was chosen randomly using a Gaussian distribution for each particle simulated.

### Mean residence time

Mean residence times for a molecule inside an RBC for the different volumes and orientations used were calculated based on the time taken for 10,000 particles to exit the

RBC, using the same simulation parameters as were used for generating the $q$-space plots. The mean residence time simulation was repeated 20 times for an RBC of 86 fl aligned with $\mathbf{B}_0$ to obtain an estimate of the statistical variance.

### Data processing

The simulated $q$-space data were interpolated using a shifting cubic spline in *Mathematica*, to increase the number of data points to 1,000 prior to generating $q$-space plots and application of the method involving the Fourier transform of the second derivative (Kuchel et al. 2004). The signal intensity was then plotted against the magnitude of the spatial wave-number vector $\mathbf{q}$ in *Mathematica* to generate a $q$-space plot, using a logarithmic scale on the ordinate to improve the visualisation of the coherence features. The $q$-space plots for gradients applied along the $x$- and $y$-axes were generated from the average of the simulated data for the two gradients.

The data from the simulations performed here contained points with negative intensity (a numerical artefact, due to the displacement distribution not extending to infinity since only $10^6$ particles were simulated), which has been noted previously (Regan and Kuchel 2002), particularly at high $q$ values, therefore the $q$-space plots were truncated at a $q$ value of $3 \times 10^5$ or $5 \times 10^5$ m$^{-1}$. The mean displacement obtained from the Fourier transform of the second derivative is dependent on the maximum value of $q$ in the data set. Therefore, in order to obtain reliable estimates of the mean displacement, the entire data series for each simulation was used. To determine if negative signal intensities interfered with the mean displacement calculated by the Fourier transform of the second derivative, the method was tested on data from a Monte Carlo simulation in a sphere (data not shown) with a diameter of 8 μm and perfectly reflecting walls. The method of the Fourier transform of the second derivative gave a mean displacement of 7.82 μm which was very close to the value (8 μm) used to describe the sphere in the first place; so it was concluded that the second derivative method was sufficiently robust to handle data with relatively minute negative intensity ($<10^{-6}$ of maximum).

### Mean length of a chord

The mean length of a chord in each of the $x$-, $y$- and $z$-directions in an RBC of a range of volumes and orientations was obtained by choosing a random point inside the model cell and calculating the length of the chord passing through the point to the boundary in the $x$-, $y$- and $z$-directions. A rotation about the $z$-axis was used to average the profile of the cell in the $x$- and $y$-directions using the method described for the diffusion simulations. This was performed for one million points for each orientation and volume, and mean values were calculated for the $x$/$y$- and $z$-directions.

## Results

### Red cell volume distribution

The mean MCV and RDW for the sample of RBCs were 84.8 fl and 12.4%, respectively. Using these values, a calculated standard deviation in the red cell volume for this sample was 5.3 fl; this was consistent with known literature values (Price-Jones 1929; Price-Jones et al. 1935). Therefore, the choice of 5 fl as the standard deviation for the simulation involving RBCs with random volume was deemed to be justified.

### Variation of cell orientation

The $q$-space plots for simulations where the orientation of the cell with respect to $\mathbf{B}_0$ was changed are shown in Fig. 2. The plot for gradients applied along the $x$/$y$-axes (Fig. 2a) showed a gradual progression from a curve without any diffraction minima for cells aligned with $\mathbf{B}_0$ and at $\theta = 10°$ to a curve with a broad minimum at $q = 2.0 \times 10^5$ m$^{-1}$ for $\theta = 45°$. This minimum shifted progressively towards lower $q$ values for $\theta = 60°$ and 90°. The plot derived for the case where the gradients were applied along the $z$-axis (Fig. 2b) showed the opposite trend, with clearly a defined minimum at $\theta = 0°$ and 10° which shifted to higher $q$ values as $\theta$ was increased, with the minimum disappearing when $\theta = 60°$.

The $q$-space plots for the simulation with RBCs given a random orientation angle $\theta$ between 0° and 6° are shown in Fig. 3. For gradients applied along the $x$/$y$-axes (Fig. 3a), the $q$-space plot showed no significant features, in a way that was similar to the $q$-space plot for cells aligned with the magnetic field, or oriented at 10° to it. The $q$-space plot for gradients applied along the $z$-axis (Fig. 3b) closely followed that for aligned cells with the most significant feature of the plot being the appearance of the first diffraction minimum at a higher $q$ value than that observed for aligned cells. This diffraction minimum was broader in the randomly oriented cells.

### Variation of cell volume

Figure 4 shows the $q$-space plots generated by simulations with cells of 76, 86 and 96 fl. When gradients were applied along $x$/$y$-direction, the $q$-space plots were featureless and showed little variation with the change in RBC volume.

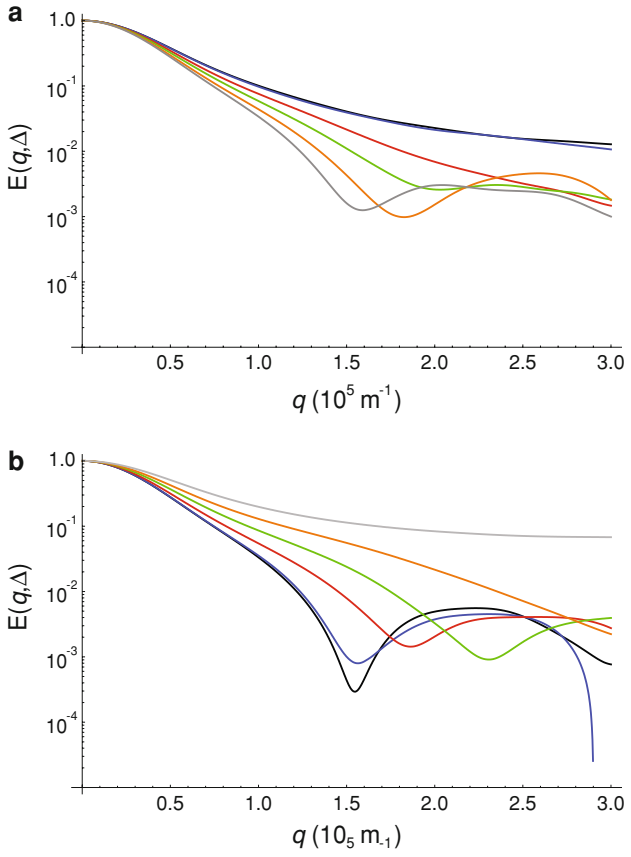


**Fig. 2** $q$-Space plots from simulations of the diffusion of water in RBCs with different orientation angle ($\theta$) with respect to $\mathbf{B}_0$. **a** Shows the plot for the average signal intensity when the magnetic field gradients were applied along the $x$- and $y$-axes, while **b** shows the plot for gradients applied along the $z$-axis. Key: *black* $\theta = 0$ (cells aligned with $\mathbf{B}_0$), *blue* $\theta = 10°$, *red* $\theta = 30°$, *green* $\theta = 45°$, *orange* $\theta = 60°$, and *grey* $\theta = 90°$

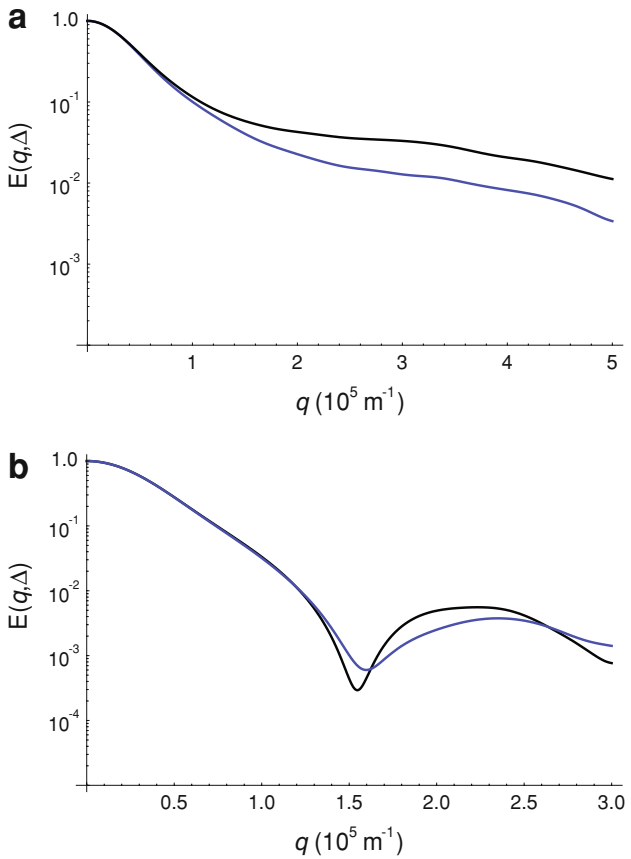


**Fig. 3** $q$-Space plots from simulations of water diffusion in RBCs when the orientation ($\theta$) of the cells was either fixed at 0° (*black lines*) or randomly chosen to be between 0° and 6° (*blue lines*), for gradients applied along, **a** the $x$- and $y$-axes, and **b** the $z$-axis

The plot for $z$-axis gradients showed a shift of the first diffraction minimum from $q = \sim 1.7 \times 10^5$ m$^{-1}$ for 76 fl cells to $q = \sim 1.4 \times 10^5$ m$^{-1}$ for 96 fl cells.

Three separate simulations of RBCs with a random volume were performed, and the $q$-space plots for each are given in Fig. 5a. The most obvious difference between the three curves was the position of the first diffraction minimum, which appeared at a different $q$ value for each set of data. The minimum was also quite broad in two of the curves. The data from the three simulations were averaged to produce a single data set for comparison with data from simulations using cells of 86 fl (Fig. 5b, c). The curves for gradients applied along the $x$- and $y$-axes were also featureless and appeared similar, except for the slightly greater attenuation in the simulation with random RBC volume. For gradients applied along the $z$-axis, the curves overlapped until the first diffraction minimum, which occurred at the same $q$ value for both the 86 fl and random-volume cells. The minimum of the $q$-space plot from random-volume cells was significantly broadened, however, and had a tail extending towards higher $q$ values.

## Mean residence time

Mean residence time data for a water molecule diffusing inside RBCs with different cell orientations are given in Table 1; and also for cells of different volume in Table 2. The standard deviation of the 20 repeated simulations was 0.1 ms, and the maximum and minimum estimates of mean residence time were 12.1 and 11.7 ms, respectively.

## Mean displacement

Mean chord length data, together with the average displacement data obtained from the Fourier transform of the second derivative, are given in Table 1 for RBCs of different orientations; and in Table 2 for RBCs of different volumes. The mean chord length along the $z$-axis for cells of 86 fl was consistent with that calculated previously using the same RBC model (Kuchel et al. 2004).

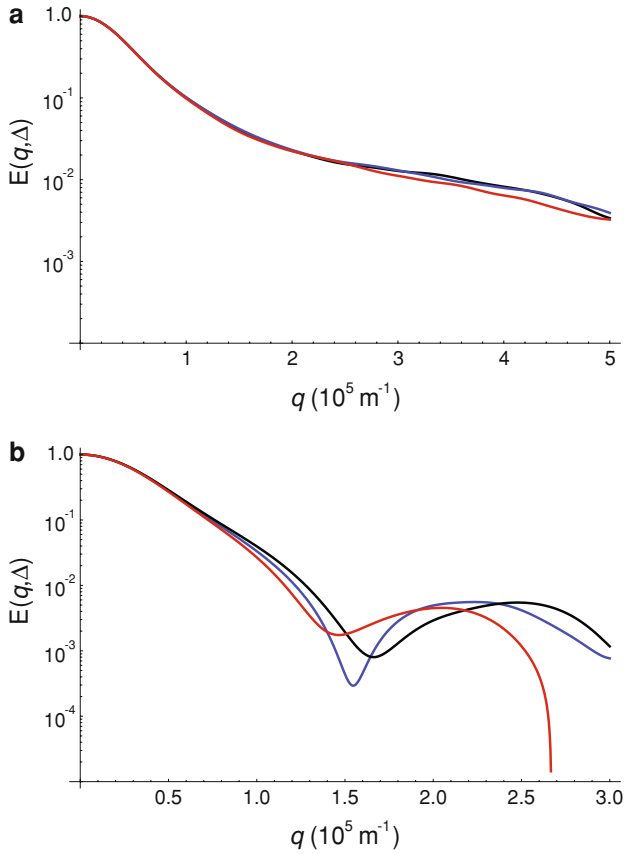


**Fig. 4** *q*-Space plots from simulations of the diffusion of water in RBCs with different volumes ($V_{cell}$). **a** Shows plots obtained when gradients were applied along the *x*- and *y*-axes, while **b** shows plots for gradients applied along the *z*-axis. Key: *black* $V_{cell} = 76$ fl, *blue* $V_{cell} = 86$ fl, *red* $V_{cell} = 96$ fl

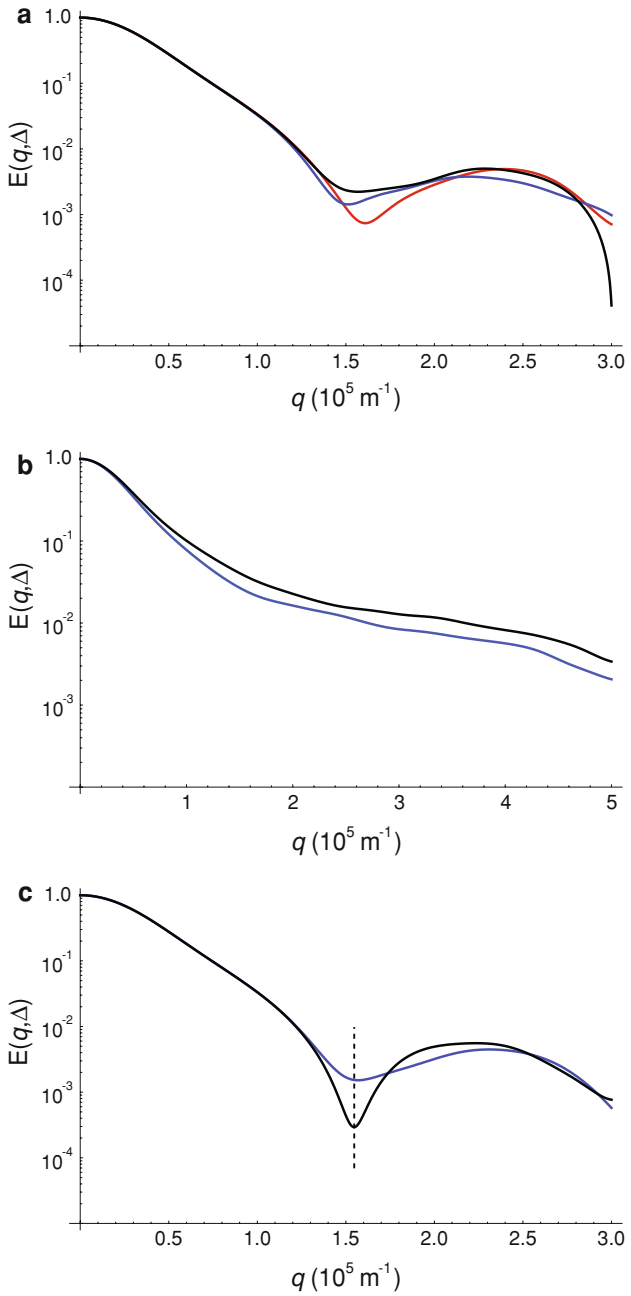


**Fig. 5** *q*-Space plots from simulations of the diffusion of water in RBCs when the volume ($V_{cell}$) of the cells was either fixed at 86 fl or randomly chosen from a normal distribution of mean 86 fl and standard deviation 5 fl. **a** Shows *q*-space plots when gradients were applied along the *z*-axis for three separate simulations with RBCs of random volume. **b** Shows the plot obtained when gradients were applied along the *x*- and *y*-axes for cells with a volume fixed at 86 fl (*black*), and for the average of the three separate simulations with random volume (*blue*). **c** Shows *q*-space plots from the same simulations as in **b** but for the situation when the gradient was applied along the *z*-axis; again the *black line* is for 86 fl cells while the *blue line* shows the results for cells with random volume

## Discussion

*q*-Space plots derived from a sample of RBCs in which the magnetic field gradients were applied in the *x*/*y*-directions and the *z*-direction, as the orientation of the cells were varied, are shown in Fig. 2. The shape of the *q*-space plots for cells where $\theta = 0°$, 45° and 90° correlates well with those shown by Jiang et al. (2001) who approximated the RBC shape as a cylinder, with a shift in the position of the first minimum towards higher *q* values for cells at 45°, and the absence of a minimum at 90°. The data in Fig. 2 showed that the troughs containing the diffraction minima were significantly broader when the gradients were applied along the *x*/*y*-axes. The rotation of the RBC about the *z*-axis generated a range of cell profiles along these axes, as seen in the mean chord length data, and this was concluded to be the cause of the broadening. The positions of the first diffraction minima when the gradients were applied along

**Table 1** Mean chord length, mean displacement, and mean residence time data from simulations of water diffusion in RBCs with various cell orientations

| Cell orientation ($\theta$, °) | Mean chord length, $x/y$ (μm) | Mean chord length, $z$ (μm) | Mean displacement, $x/y$ (μm) | Mean displacement, $z$ (μm) | Mean residence time (ms) |
|---|---|---|---|---|---|
| 0 | 2.95 | 5.83 | 1.17 | 5.87 | 11.9 ± 0.1 |
| 10 | 2.97 | 5.14 | 1.17 | 5.87 | 11.7 ± 0.1 |
| 30 | 3.18 | 3.06 | 3.52 | 5.87 | 12.1 ± 0.1 |
| 45 | 3.53 | 2.38 | 4.70 | 4.70 | 12.0 ± 0.1 |
| 60 | 4.13 | 2.04 | 4.70 | 3.52 | 11.8 ± 0.1 |
| 90 | 5.83 | 1.82 | 7.04 | 1.17 | 11.7 ± 0.1 |
| Random | 2.95 | 5.71 | 1.17 | 5.87 | 11.9 ± 0.1 |

Mean chord lengths are given for $x/y$- and $z$-directions. Mean displacement values were determined using the method that involves the Fourier transform of the second derivative of the $q$-space data. The mean residence time is given as the mean ± SD, based on 20 repeated simulations for RBCs at 0°

**Table 2** Mean chord length, mean displacement, and mean residence time data from simulations of water diffusion in RBCs with various cell volumes

| Cell volume (fl) | Mean chord length, $x/y$ (μm) | Mean chord length, $z$ (μm) | Mean displacement, $x/y$ (μm) | Mean displacement, $z$ (μm) | Mean residence time (ms) |
|---|---|---|---|---|---|
| 76 | 2.89 | 5.45 | 1.17 | 5.87 | 11.8 ± 0.1 |
| 86 | 2.95 | 5.83 | 1.17 | 5.87 | 11.9 ± 0.1 |
| 96 | 3.01 | 6.16 | 1.17 | 7.05 | 12.1 ± 0.1 |
| Random | 2.95 | 5.83 | 1.17 | 5.87 | 11.8 ± 0.1 |

Mean chord lengths are given for $x/y$- and $z$-directions. Mean displacement values were determined using the method that involves the Fourier transform of the second derivative of the $q$-space data. The mean residence time is given as the mean ± SD, based on 20 repeated simulations for RBCs of 86 fl

the $z$-axis, for cells aligned with $\mathbf{B}_0$, and for gradients applied along the $x/y$-axes for cells perpendicular to $\mathbf{B}_0$, appeared at the same value of $q$. This reflects the almost identical profile of the cell when it is projected along these axes in both situations. The trend in the position of the first diffraction minimum in the $q$-space plots is reflected in the data describing the mean chord length (Table 1), with the mean lengths decreasing along $z$, and increasing along $x/y$ as the orientation of the RBCs changed.

The mean displacement data generated from the Fourier transformation of the second derivative of the $q$-space data were not consistent with the mean chord length data obtained with most of the cell orientations. The notable exception was the displacement along $z$, for cells aligned with $\mathbf{B}_0$ where there was good agreement between both values of the mean displacement and mean chord length. The method involving the Fourier transform of the second derivative was able to distinguish between cells of different orientations providing there was a difference in $\theta$ of at least 15–30°, but it had poor discrimination power when the angle was less than this.

The appearance of the first diffraction minimum at a higher $q$ value for RBCs with a random orientation was reflected in the smaller mean chord length in the $z$-direction for randomly oriented cells, compared with aligned cells. As with the other simulations involving changing the orientation of the RBCs, the Fourier transform of the second derivative could not discriminate between cells aligned with the magnetic field and those with a random orientation.

The mean residence times of a particle (water molecule) inside the RBC calculated here were consistent with those reported previously (Regan and Kuchel 2000), and with literature values for RBCs obtained from manganese doping (Benga et al. 1990), and PGSE (Andrasko 1976) experiments at 25°C. No dependence on the orientation of the RBCs was seen, as all values fell between the maximum and minimum values obtained from 20 repeated estimates of the mean residence time in an RBC of 86 fl aligned with $\mathbf{B}_0$.

Changing the volume of the RBCs had no significant effect on the shape of the $q$-space plots when gradients were applied along the $x/y$-axes, with the lines of the graph overlapping in the plot (Fig. 4a); this feature is reflected in the small change in mean chord length reported in Table 2. The lack of difference in the curves can be attributed to the averaging effect of the rotation of the cells about the $z$-axis. The $q$-space plot derived when the gradients were applied

along the $z$-axis showed the first diffraction minimum at a significantly different $q$ value (Fig. 4b); this corresponded well with the changes in mean cord length reported in Table 2. As with the simulations where the orientation of the cell was changed, the data-processing method that uses the Fourier transform of the second derivative failed to discriminate between cells of different volumes.

The three simulations performed with identical experimental parameters, but with cells of randomly assigned volumes, showed differences in the position of the first diffraction minimum in the resulting $q$-space plots (Fig. 5a); this reflected the randomness with which the volumes were assigned. The differences between the $q$-space plots give an indication of the variations expected in real experiments. When the average signal intensities from the three random-volume simulations were compared with the data from cells with a volume of 86 fl, the first minimum occurred at the same value of $q$ (Fig. 5c); however, the diffraction minimum for RBCs of random volume became broader and more closely resembled $q$-space plots that have been acquired from real samples of RBCs (Kuchel et al. 1997; Pages et al. 2008).

In conclusion, the present work has extended the model used previously by us to simulate the diffusion of water in RBCs (Regan and Kuchel 2000, 2002, 2003a, b), to include the effects of variable orientation and volume of the cells. The results of the simulations carried out here showed that features of $q$-space plots from RBCs, particularly the position of the first diffraction minimum, were dependent both on the cell orientation and cell volume. However, unlike the previous studies on diffusion in cylinders (Avram et al. 2004, 2008), no strong angular dependence of the signal attenuation was seen in the present work, with diffraction minima seen for RBC orientations up to 45°. The dependence of the $q$-space plots from RBCs on cellular orientation seen in our simulations could be confirmed using a triple axis gradient probe to apply gradients in any direction across a suspension of RBCs. Sufficient magnetic field-gradient strength would be needed to incur sufficient signal attenuation to manifest diffusion-coherence features.

**Acknowledgments** We thank Dr Bob Chapman for discussions regarding the programming, and Dr Guilhem Pages for assistance with the implementation of the second derivative method and discussions regarding $q$-space plots from suspensions of erythrocytes. The work was funded by a Discovery grant from the Australian Research Council to PWK and Dr Jamie Vandenberg. TJL was supported by a University of Sydney Postgraduate Award.

## References

Andrasko J (1976) Water diffusion permeability of human erythrocytes studied by a pulsed gradient NMR technique. Biochim Biophys Acta 428:304–311

Avram L, Assaf Y, Cohen Y (2004) The effect of rotational angle and experimental parameters on the diffraction patterns and micro-structural information obtained from q-space diffusion NMR: implication for diffusion in white matter fibers. J Magn Reson 169:30–38. doi:10.1016/j.jmr.2004.03.020

Avram L, Ozarslan E, Assaf Y, Bar-Shir A, Cohen Y, Basser PJ (2008) Three-dimensional water diffusion in impermeable cylindrical tubes: theory versus experiments. NMR Biomed 21:888–898. doi:10.1002/nbm.1277

Benga G, Pop VI, Popescu O, Borza V (1990) On measuring the diffusional water permeability of human red blood cells and ghosts by nuclear magnetic resonance. J Biochem Biophys Methods 21:87–102. doi:10.1016/0165-022X(90)90057-J

Callaghan PT (1997) A simple matrix formalism for spin echo analysis of restricted diffusion under generalized gradient waveforms. J Magn Reson 129:74–84. doi:10.1006/jmre.1997.1233

Callaghan PT, Coy A, Macgowan D, Packer KJ, Zelaya FO (1991) Diffraction-like effects in NMR diffusion studies of fluids in porous solids. Nature 351:467–469. doi:10.1038/351467a0

Cory DG, Garroway AN (1990) Measurement of translational displacement probabilities by NMR—an indicator of compartmentation. Magn Reson Med 14:435–444. doi:10.1002/mrm.1910140303

Dacie JV, Lewis SM (1975) Practical haematology, 5th edn. Churchill Livingstone, Edinburgh

Jiang PC, Yu TY, Perng WC, Hwang LP (2001) Pore-to-pore hopping model for the interpretation of the pulsed gradient spin echo attenuation of water diffusion in cell suspension systems. Biophys J 80:2493–2504. doi:10.1016/S0006-3495(01)76221-2

Kuchel PW, Fackerell ED (1999) Parametric-equation representation of biconcave erythrocytes. Bull Math Biol 61:209–220. doi:10.1006/bulm.1998.0064

Kuchel PW, Coy A, Stilbs P (1997) NMR "diffusion-diffraction" of water revealing alignment of erythrocytes in a magnetic field and their dimensions and membrane transport characteristics. Magn Reson Med 37:637–643. doi:10.1002/mrm.1910370502

Kuchel PW, Durrant CJ, Chapman BE, Jarrett PS, Regan DG (2000) Evidence of red cell alignment in the magnetic field of an NMR spectrometer based on the diffusion tensor of water. J Magn Reson 145:291–301. doi:10.1006/jmre.2000.2093

Kuchel PW, Eykyn TR, Regan DG (2004) Measurement of compartment size in q-space experiments: Fourier transform of the second derivative. Magn Reson Med 52:907–912. doi:10.1002/mrm.20219

Mansfield P, Grannell PK (1973) NMR diffraction in solids. J Phys C Solid State Phys 6:L422–L426. doi:10.1088/0022-3719/6/22/007

Pages G, Szekely D, Kuchel PW (2008) Erythrocyte-shape evolution recorded with fast-measurement NMR diffusion-diffraction. J Magn Reson Imaging 28:1409–1416. doi:10.1002/jmri.21588

Price-Jones C (1929) Red cell diameters in one hundred healthy persons and in pernicious anaemia: the effect of liver treatment. J Pathol Bacteriol 32:479–501. doi:10.1002/path.1700320312

Price-Jones C, Vaughan JM, Goddard HM (1935) Haematological standards of healthy persons. J Pathol Bacteriol 40:503–519. doi:10.1002/path.1700400309

Regan DG, Kuchel PW (2000) Mean residence time of molecules diffusing in a cell bounded by a semi-permeable membrane: Monte Carlo simulations and an expression relating membrane transition probability to permeability. Eur Biophys J 29:221–227. doi:10.1007/s002490000081

Regan DG, Kuchel PW (2002) Simulations of molecular diffusion in lattices of cells: Insights for NMR of red blood cells. Biophys J 83:161–171. doi:10.1016/S0006-3495(02)75158-8

Regan DG, Kuchel PW (2003a) Simulations of NMR-detected diffusion in suspensions of red cells: the "signatures" in q-space

plots of various lattice arrangements. Eur Biophys J 31:563–574

Regan DG, Kuchel PW (2003b) Simulations of NMR-detected diffusion in suspensions of red cells: the effects of variation in membrane permeability and observation time. Eur Biophys J 32:671–675. doi:10.1007/s00249-003-0331-x

Söderman O, Jonsson B (1995) Restricted diffusion in cylindrical geometry. J Magn Reson A 117:94–97. doi:10.1006/jmra.1995.0014

Stejskal EO, Tanner JE (1965) Spin diffusion measurements: spin echoes in the presence of a time-dependent field gradient. J Chem Phys 42:288–292. doi:10.1063/1.1695690

Torres AM, Taurins AT, Regan DG, Chapman BE, Kuchel PW (1999) Assignment of coherence features in NMR q-space plots to particular diffusion modes in erythrocyte suspensions. J Magn Reson 138:135–143. doi:10.1006/jmre.1998.1701